Science Advances
AAAS

Supplementary Materials for

Neuroserpin and transthyretin are extracellular chaperones that preferentially inhibit amyloid formation

Jennifer West, Sandeep Satapathy, Daniel R. Whiten, Megan Kelly, Nicholas J. Geraghty, Emma-Jayne Proctor, Pietro Sormanni, Michele Vendruscolo, Joel N. Buxbaum, Marie Ranson, Mark R. Wilson*

*Corresponding author. Email: mrw@uow.edu.au

Published 10 December 2021, *Sci. Adv.* **7**, eabf7606 (2021)
DOI: 10.1126/sciadv.abf7606

This PDF file includes:

Supplementary Information

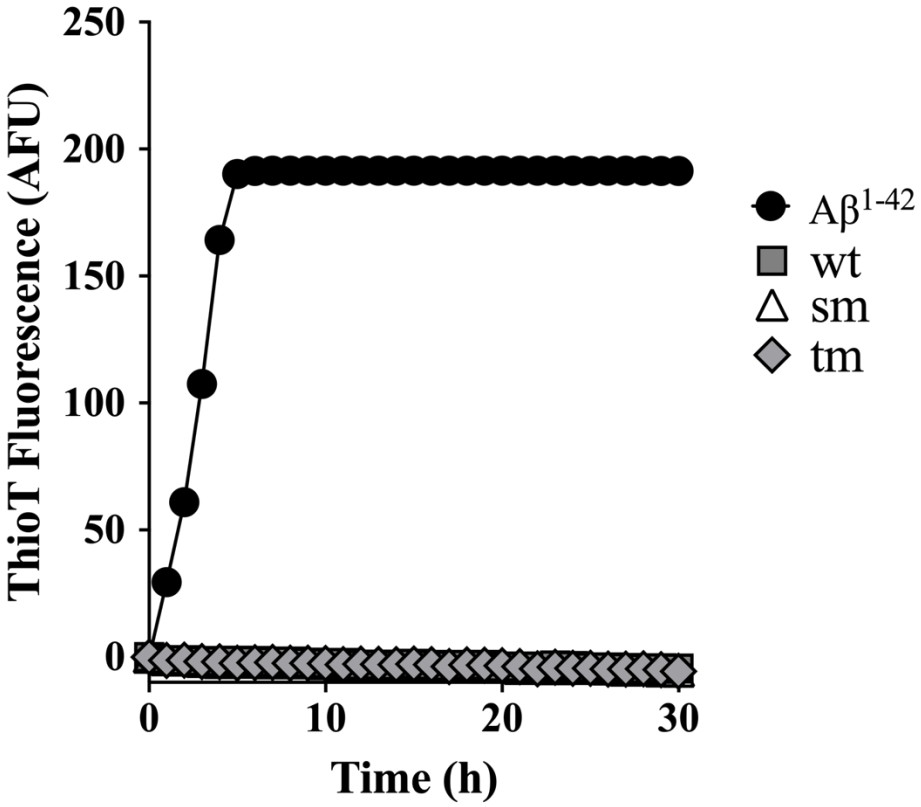

Supplementary Figure 1 NS^{wt} (wt), NS^{sm} (sm) and NS^{tm} (tm) generate negligible ThioT fluorescence when incubated alone under the conditions used in $A\beta^{1-42}$ aggregation assays. Data points plotted represent means of triplicate measurements; SE are plotted but are too small to be visible. Similar results were obtained under the conditions used for ccβω and α-syn aggregation assays.

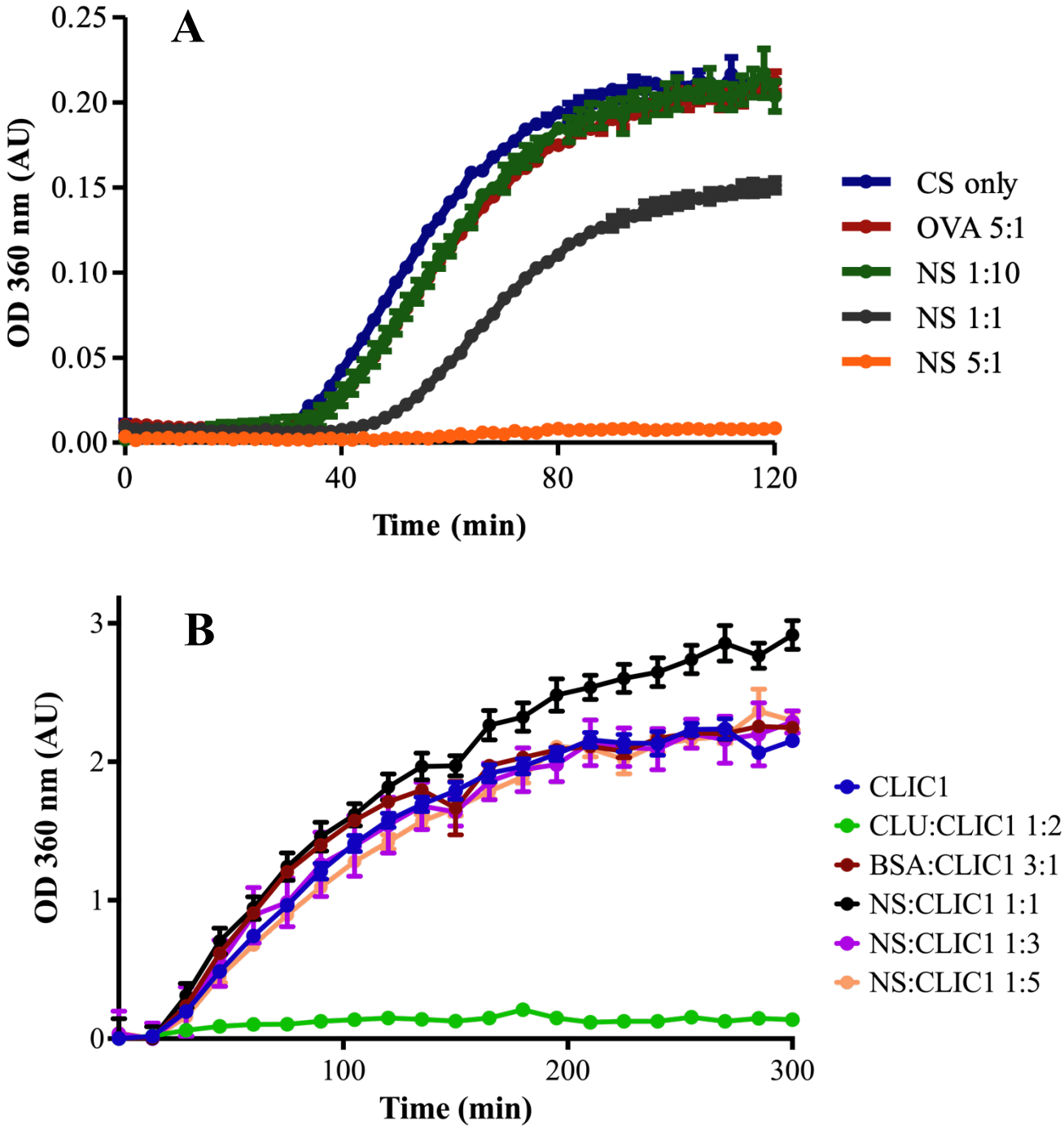

Supplementary Figures 2A&B. Effects of NS on the amorphous aggregation of CS and CLIC1. **(A)** CS (1.8 μM), either alone or supplemented with individual proteins indicated in the key, was incubated for 2 h at 43 °C to induce aggregation. (B) CLIC1 (60 μM), either alone or supplemented with the individual proteins indicated in the key, was incubated at 37 ºC for 5 h to induce aggregation. The molar ratios of test protein:CS or test protein:CLIC1 are indicated in the respective keys. In both cases, protein aggregation was measured as turbidity, recorded as optical density (OD) at 360 nm, in absorbance units (AU) as a function of time. Data points are the mean of triplicate measurements ± SEM and the results shown are each representative of two independent experiments. In some cases, the error bars are too small to be visible.

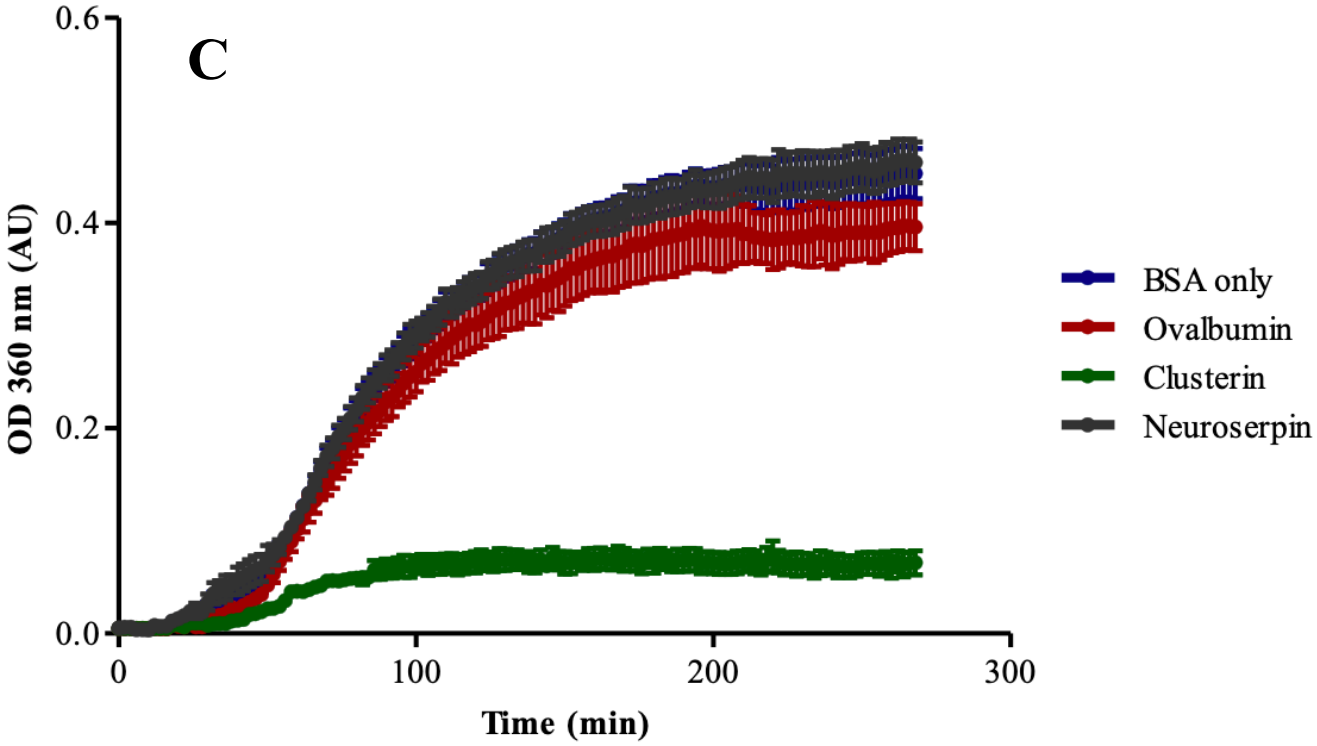

Supplementary Figure 2C. NS did not inhibit the reduction-induced amorphous aggregation of BSA. BSA (10 μM) was incubated with 20 mM DTT for 5 h at 37°C and aggregation measured as turbidity at 360 nm. Each of the test proteins (indicated in key) were present at a molar ratio of test protein:BSA = 1:2. Data points are the mean of triplicate measurements ± SEM and the results shown are representative of two independent experiments.

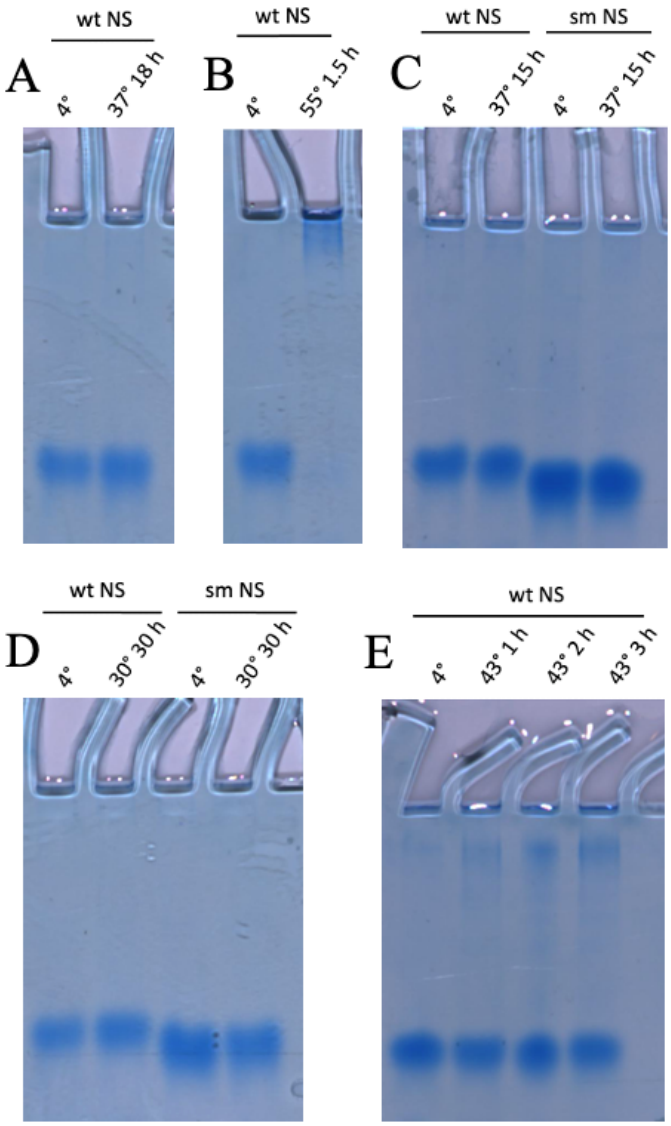

Supplementary Figure 3 The conditions used for protein aggregation assays induce no detectable, or very limited, polymerization of NS. Images of native polyacrylamide gels, analysing the effects of various incubation conditions on wild type (wt) NS and single mutant (sm) NS. In all cases, 10 µg of NS protein was loaded into each lane (protein identity and treatments indicated above respective lanes). **(A)** Incubation of wt NS for 18 h at 37 ºC (corresponding to Figures 2B&C) had no visible effect on its migration in native gel electrophoresis (NGE), however **(B)** extensive polymerization of wt NS was induced when the protein was incubated at 55 ºC for 1.5 h (this extreme condition does not correspond with any used in protein aggregation assays presented in this manuscript). **(C)** Incubation of wt and sm NS at 37 ºC for 15 h (considerably longer than the 6 h at 37 ºC used to produce the results shown in Figure 7B) had no visible effect on the migration of either protein in NGE. sm NS migrates slightly faster than wt NS under these conditions. **(D)** Incubation of wt and sm NS at 30 ºC for 30 h (corresponding to Figures 2A & 7A) had no visible effect on the migration of either protein in NGE. **(E)** Incubation of wt NS at 43 ºC, conditions used in the amorphous aggregation of CS, induced detectable but very limited polymerization of wt NS (represented by the relatively faint band towards the top of the gel). Mutant NS was not tested in amorphous protein aggregation assays. All incubations were performed in PBS, except those shown in (E) which were performed in the buffer used in CS aggregation assays (50 mM Tris-HCl, 5 mM Hepes, pH 8.0). Results shown are each representative of at least two independent experiments.

Supplementary Figure 4. PyMOL-generated structure of an NS dimer showing the 14-residue homologous region (depicted in red), which is positioned distant from the dimer interface.

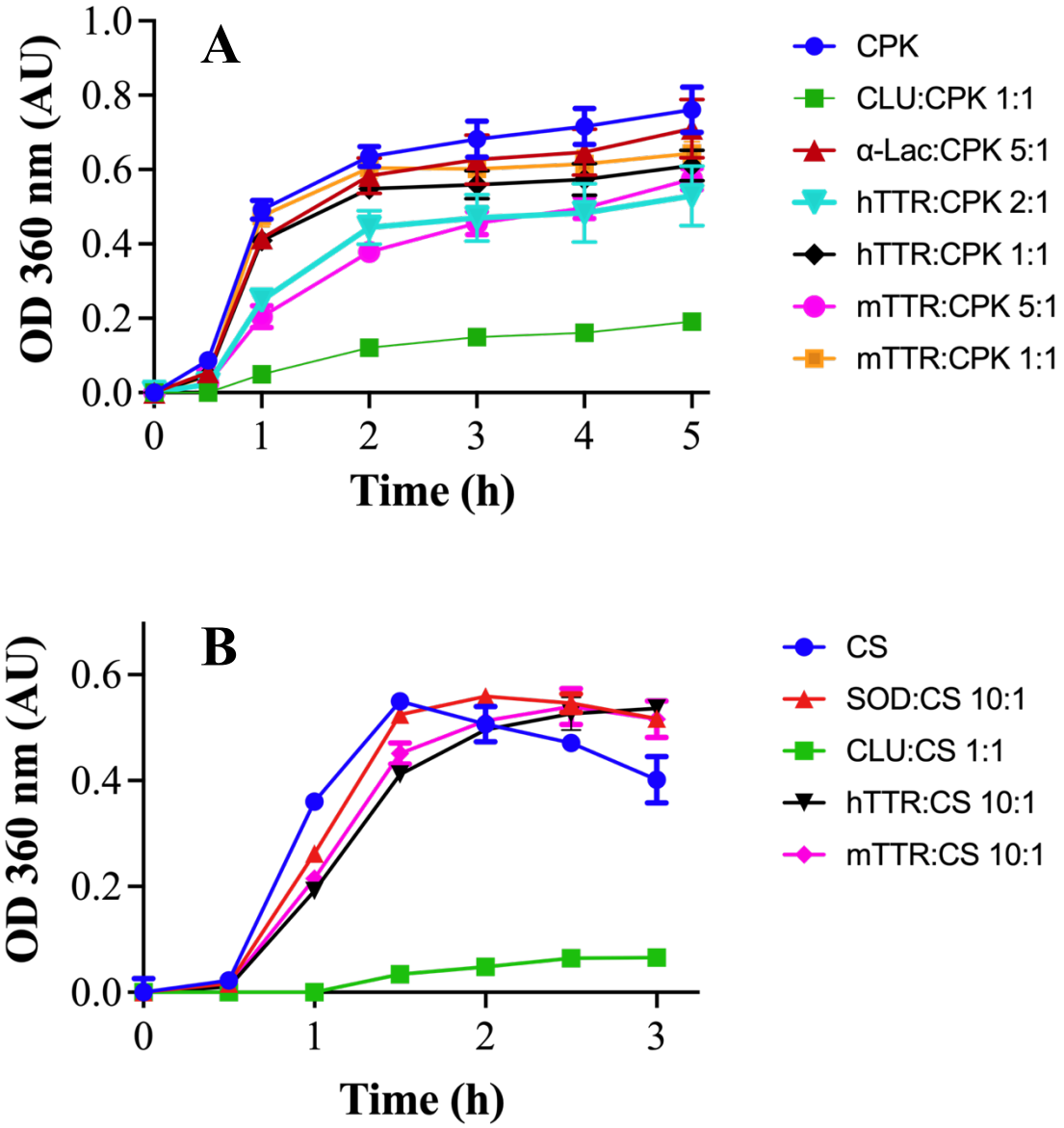

Supplementary Figure 5. Effects of hTTR and mTTR on the heat-induced aggregation of CPK and CS. (**A**) CPK (15 μM), either alone or supplemented with individual proteins indicated in the key, was incubated at 43°C for 5 h to induce aggregation. α-Lactalbumin (α -Lac) was used as a non-chaperone control protein. (**B**) CS (1.8 μM), incubated either alone or supplemented with individual proteins indicated in the key, was incubated at 43°C for 3 h to induce aggregation. Superoxide dismutase 1 (SOD) was used as a non-chaperone control protein. In both (A) and (B), clusterin (CLU) was used as a known chaperone protein expected to inhibit aggregation of the client protein, and protein aggregation was measured as turbidity, recorded as optical density (OD) at 360 nm, in absorbance units (AU) as a function of time. Data points are the mean of triplicate measurements ± SEM and the results shown are each representative of two independent experiments. In some cases, the error bars are too small to be visible. In (B), the reduction in OD 360 nm for CS alone between 1.5-3 h is attributable to "settling" of large aggregates in the wells, which we have noted occurs with some batches of CS. For this reason, in this case, comparisons between OD for the various samples were made at 1.5 h (see Figure 5D).

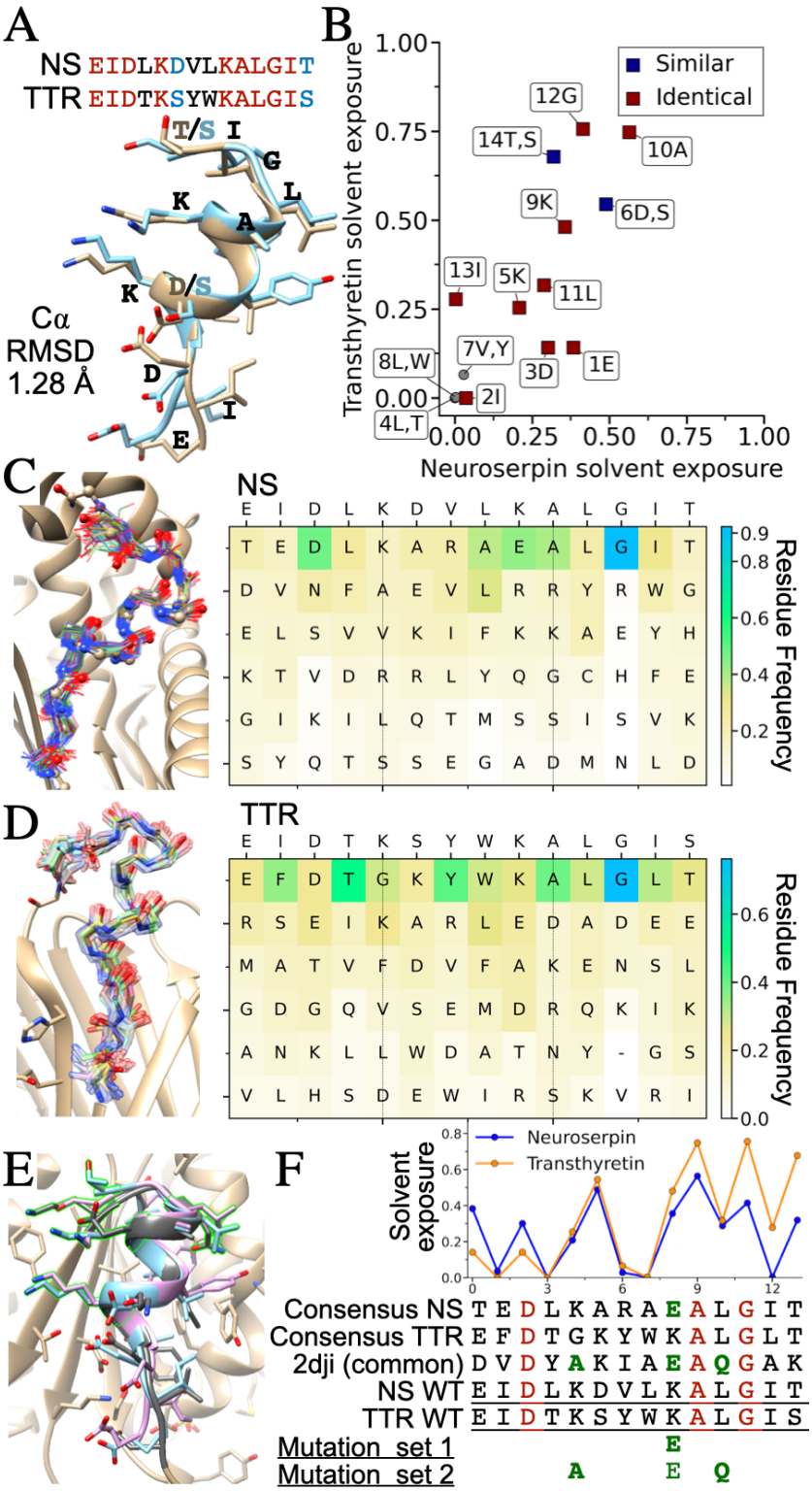

Supplementary Figure 6 Rational design of NS mutants. (A) Sequence alignment and structural superimposition of the putative anti-amyloid motif with TTR in light blue and NS in light brown. Identical residues are in red and similar ones in blue (i.e. those with blosum62 score greater or equal than zero). The root mean square deviation (RSMD) for the distance between the α–carbon (Cα) atoms in this alignment is 1.28 Å. (B) Scatter plot of solvent exposure of amino acids belonging to the motif within the native structures of transthyretin (y-axis) and neuroserpin (x-axis). Solvent exposure for amino acid X is calculated with respect to the solvent-accessible surface area of X in the

context of an extended Gly-X-Gly 3-peptide. All residues highly exposed to the solvent (exposure >~ 0.25), which are those most likely to engage with the substrate, are either identical (red squares) or similar (blue squares), while more different residues (grey dots) are not exposed and are likely involved in structural contacts with the protein core. (C, D) Structural alignment of the putative anti-amyloid motif with structurally similar motifs (Cα RMSD ≤ 0.75 Å) from the PDB90 database. (C) The structure of the NS motif is shown to the left superimposed with 142 structurally similar hits (73 unique sequences), and the corresponding residue frequency is represented on the right with residues at each position sorted from the most frequent at the top and coloured according to their observed frequency (colour-bar); the sequence above the plot is that of the NS motif. (D) Same as (C) but for transthyretin, for which the search returned 79 hits corresponding to 32 unique sequences. (E) Structure of bacterial pyruvate oxidase (PDB 2dji) coloured in light brown; this protein represents the only hit in common between the NS and TTR alignments shown in panels C and D. The matching motif is shown in dark grey and is structurally aligned to the NS (light blue) and TTR (pink) motifs. Candidate mutation sites are highlighted in green. (F) Designed mutations were identified by combining together information relating to residue solvent exposure, residue identity within the NS, TTR and 2dji motifs, and amino acid frequencies from the sequences of the structurally similar motifs (C, D). Amino acids coloured in red are fully conserved positions that are likely to be crucial for preserving the structural integrity of the motif. Selected mutations are coloured in green.

Methods to rationally design NS mutants

To verify whether or not the identified 14-residue putative anti-amyloid motif is indeed the source of the observed anti-amyloid activity, we rationally designed a set of mutations at solvent-exposed sites that are identical in NS and TTR. The goal was to select residue substitutions with the highest likelihood of disrupting the anti-amyloid activity, while preserving the structural integrity of the motif. Therefore, substitutions were carried out to amino acids with very different sidechain chemistry, but that were expected to have no effect on the structure.

Specifically, we first analysed the motif in the context of the native structures of NS and TTR (Supplementary Figures 6A&B). This analysis revealed that those residues that are most solvent-exposed in the native states, and hence most likely to interact with the amyloidogenic substrates, are either identical or chemically-similar in the two proteins, as would be expected from a functionally-relevant structural motif. Supplementary Figure 6B shows that there are six sites that are more than 25% solvent-exposed in both proteins, and hence likely to be involved in functional interactions.

To narrow down this list of candidate mutation sites, and to select those mutations least likely to affect the structure of the motif, we searched the PDB90 database for structurally-similar motifs. The PDB90 contains all structures from the Protein Data Bank with less than 90% sequence identity, and we searched it for structural motifs of the same length (14 residues) by using the MASTER program (52) with a Cα atom RMSD cut-off of 0.75 Å. This structural search was carried out by using as query both the NS and TTR motifs (Supplementary Figures 3C&D).

The analysis of the amino acid sequences forming these structurally-similar motifs revealed that positions D3, A10, and especially G12 are likely to play an important role in defining the structure of the motif, as they are highly conserved among the structurally similar motifs identified (Supplementary Figure 6C). These sites were therefore removed from the list of candidate mutation sites. Moreover, as the Cα RMSD between the NS and TTR motifs is 1.28 Å, the search was carried out with a RMSD cutoff of 0.75 Å and yielded only one fragment that is structurally-similar to both motifs (residues 493-506 of PDB 2dji chain A, a bacterial pyruvate oxidase, Supplementary Figure 6E).

We therefore selected a set of candidate mutations by combining information about amino acid identity between the NS and TTR motifs, their residue solvent-exposure, the amino acid frequencies and consensus sequences of structurally similar motifs, and the sequence of the 2dji motif, as this represents a 'structural intermediate' between the two motifs. Supplementary Figure 6F shows that the first choice mutation to test was K9E, as this is a solvent-exposed site with a lysine in both NS and TTR, which suggests it is likely to be functionally important for anti-amyloid activity. Conversely, a glutamate is found at this site in the 2dji motif as well as in the consensus sequence of motifs structurally similar to the NS one, while it is second-ranking among those structurally similar to TTR. Taken together, these observations suggest that a glutamate will preserve the structural integrity of the NS motif, while the charge reverse brought about by this substitution is likely to have a large impact on anti-amyloid activity. Other possible mutations identified with this strategy are K5A and L11Q, as (i) these substitutions change substantially the sidechain chemistry and thus are likely to impact activity; (ii) these are the amino acids found in the 2dji motif, and (iii) these sites are not particularly conserved in motifs structurally similar to that of NS, which suggest that these mutations will likely preserve the structure.

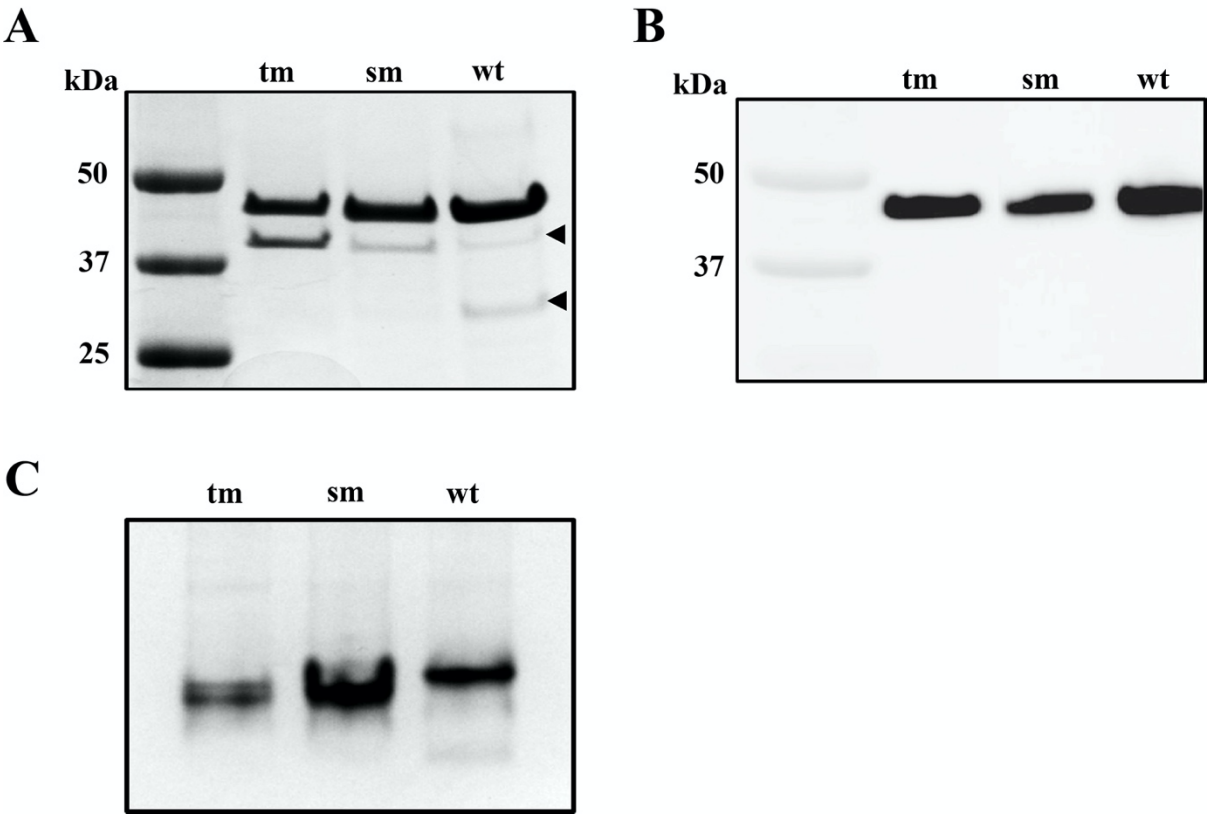

Supplementary Figure 7. Electrophoretic and immunoblotting analyses of recombinant wild type and mutant neuroserpin. (**A**) SDS PAGE analysis of purified NS^{wt} (wt), NS^{sm} (sm) and NS^{tm} (tm) under non-reducing conditions. Additional bands at ~ 40 kDa and ~33 kDa are indicated by black arrowheads and are likely to represent minor cleavage products. (**B**) Western blot of the same proteins probed with anti-6His antibody. In A and B, the molecular mass of protein standards (left) is shown in kDa. (**C**) Native gel electrophoresis of the same three NS molecules. Results are representative of three independent experiments.

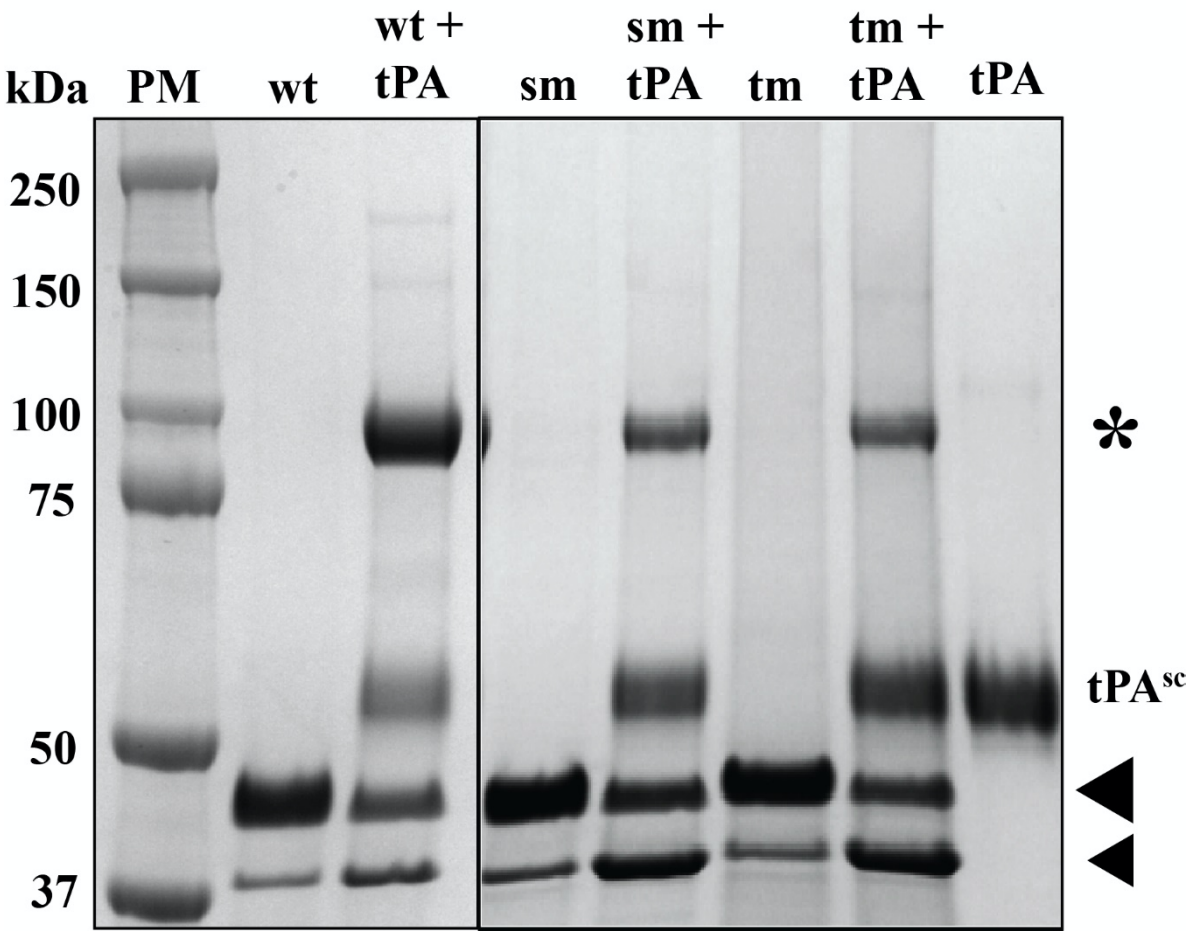

Supplementary Figure 8. Interaction of wild type and mutant NS with tPA to form covalently linked NS-tPA complexes. Composite image of Coomassie blue-stained, non-reducing 10% SDS-PAGE gels showing results of the analysis of purified wild-type NS (wt), mutant NS (sm and tm), tPA and mixtures of wt/sm/tm-NS and tPA. Molecular markers of known mass (kDa) are indicated on the left side of the image and the sample loaded into each well is indicated at the top of the image. The Acetylyse tPA preparation is mostly comprised of single-chain tPA (tPA^{sc}; indicated at right of image). Individual NS proteins resolve at ~ 46 kDa (large arrowhead). When (wt, sm or tm) NS was incubated with tPA, high molecular weight, SDS-stable species were detected (note the prominent band at ~ 95 kDa indicated by the asterisk); an increase in cleaved NS was also detected (small black arrowhead).

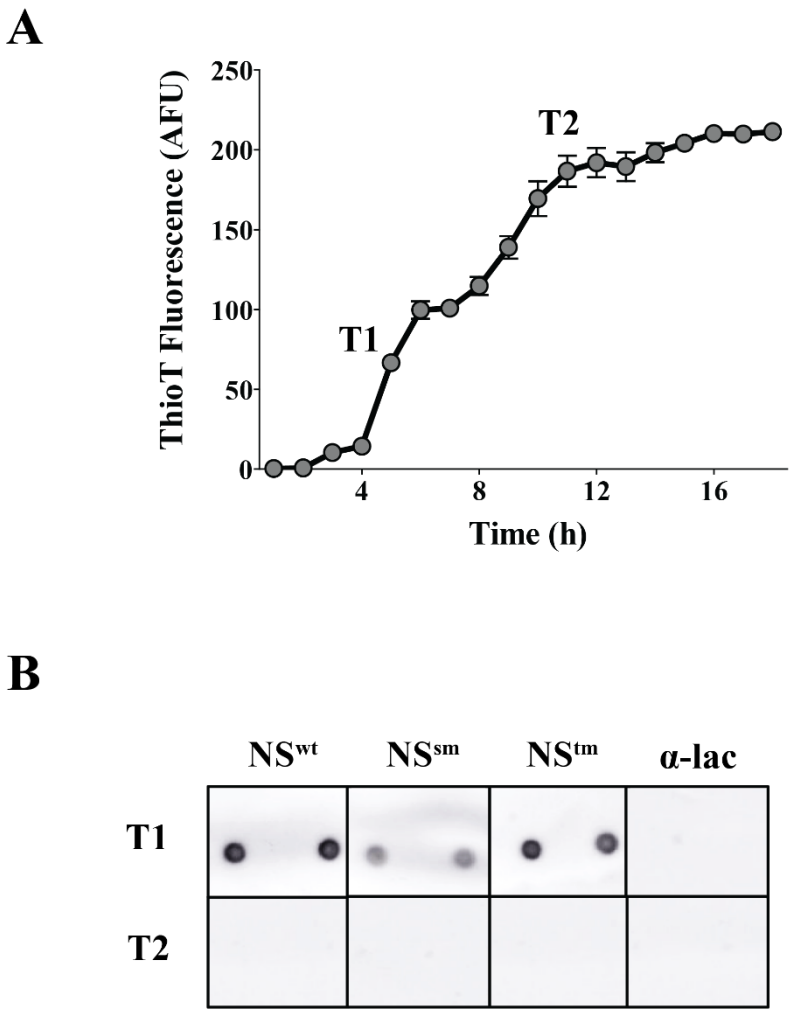

Supplementary Figure 9. Native immunodot-blot measuring the binding of biotin Aβ$^{1-42}$ to immobilized wild-type and mutant neuroserpin. (A) Samples of biotin Aβ$^{1-42}$ (purchased from Anaspec, CA, USA) were collected at 5 h (T1) and 12 h (T2) following the start of the aggregation assay, which was monitored using the time-dependent increase in ThioT fluorescence. Data points represent means +/- SEM (n=3). T1 and T2 represent presumptive early (oligomeric) and late (fibrillar) species. **(B)** 0.25 μg of NS^{wt}, NS^{sm} and NS^{tm}, and α-lactalbumin (α-lac, used as a non-chaperone control protein), were spotted onto a nitrocellulose membrane and the membrane subsequently blocked with 5% (w/v) skimmed milk in PBS (SM/PBS) for 1 h at room temperature (RT). The blot was then incubated with 40 μM biotin-Aβ$^{1-42}$ (T1 or T2) for 1 h at RT and washed twice with PBS to remove any unbound biotin-Aβ$^{1-42}$. Finally, biotin-Aβ$^{1-42}$ bound to immobilised proteins was detected using streptavidin-HRP (1:1000 dilution in SM/PBS). The blot was developed using enhanced chemiluminescence (please refer to the main text Methods section for details). Results shown are representative of 2 independent experiments.

Supplementary Figure 10. Amphipathicity of predicted NS and TTR α-helices. Helix pinwheel projections were generated to show predicted regions of hydrophobicity on the homologous α-helices corresponding to NS (left) and TTR (right). Hydrophobic residues are depicted in yellow, charged residues in blue, and polar residues in red. The residues in this figure are numbered according to their placement in the 14-mer sequence (residues 1–14). Residues L4 and L8 (NS), and T4 and W8 (TTR) are predicted to have limited solvent exposure (Supplementary Figure 6B), but the remaining residues may in each case constitute an amphipathic α-helix.

Methods to generate pinwheel structures

Alpha-helical pinwheel structures were generated by the Helical Wheel Projections tool (Don Armstrong and Raphael Zidovetzki; Version: Id: wheel.pl,v 1.4 2009-10-20 21:23:36 don Exp; University of California, Riverside, United States) using the default settings. Only residues corresponding to the α-helices within the 14-mer region of similarity were used; residues 303-310 for NS and residues 95-101 for TTR (residue numbering includes the N-terminal signal peptides in both cases). Protein sequences were obtained from UniProtKB/Swiss-Prot reviewed entries.

Supplementary Table 1. Secondary structure content predicted from far UV CD analysis of NS^{wt}, NS^{sm} and NS^{tm} (see Figure 6A).

Protein	Alpha-Helix	Beta-strand	Turn	Disordered
NS^{wt}	16.2	40.7	11	32.2
NS^{sm}	25.2	39.2	9.3	26.4
NS^{tm}	21	40.7	9.8	28.5

Supplementary Table 2. Apparent melting temperatures (Tm) for NS^{wt}, NS^{sm} and NS^{tm} measured by thermal shift assay (see Figure 6B). Values shown are means of 8 replicates and the corresponding SEM are also indicated.

Protein	Apparent Tm (ºC)	SEM (ºC)
NS^{wt}	51.8	0.06
NS^{sm}	51.3	0.1
NS^{tm}	49.3*	0.3

* Significantly different from NS^{wt} and NS^{sm} (ANOVA, Tukey's multiple comparison test, $p < 0.05$)

REFERENCES AND NOTES

1. J. J. Yerbury, E. M. Stewart, A. R. Wyatt, M. R. Wilson, Quality control of protein folding in extracellular space. *EMBO Rep.* **6**, 1131–1136 (2005).

2. A. R. Wyatt, J. Y. Yerbury, H. Ecroyd, M. R. Wilson, Extracellular chaperones and proteostasis. *Annu. Rev. Biochem.* **82**, 295–322 (2013).

3. H. M. Nielsen, L. Minthon, E. Londos, K. Blennow, E. Miranda, J. Perez, D. C. Crowther, D. A. Lomas, S. M. Janciauskiene, Plasma and CSF serpins in Alzheimer disease and dementia with Lewy bodies. *Neurology* **69**, 1569–1579 (2007).

4. E. Miranda, D. A. Lomas, Neuroserpin: A serpin to think about. *Cell. Mol. Life Sci.* **63**, 709–722 (2006).

5. H. Loebermann, R. Tokuoka, J. Deisenhofer, R. Huber, Human α1-proteinase inhibitor. Crystal structure analysis of two crystal modifications, molecular model and preliminary analysis of the implications for function. *J. Mol. Biol.* **177**, 531–557 (1984).

6. G. A. Hastings, T. A. Coleman, C. C. Haudenschild, S. Stefansson, E. P. Smith, R. Barthlow, S. Cherry, M. Sandkvist, D. A. Lawrence, Neuroserpin, a brain-associated inhibitor of tissue plasminogen activator is localized primarily in neurons. Implications for the regulation of motor learning and neuronal survival. *J. Biol. Chem.* **272**, 33062–33067 (1997).

7. M. Yepes, M. Sandkvist, T. A. Coleman, E. Moore, J. Y. Wu, D. Mitola, T. H. Bugge, D. A. Lawrence, Regulation of seizure spreading by neuroserpin and tissue-type plasminogen activator is plasminogen-independent. *J. Clin. Invest.* **109**, 1571–1578 (2002).

8. R. L. Davis, A. E. Shrimpton, P. D. Holohan, C. Bradshaw, D. Feiglin, G. H. Collins, P. Sonderegger, J. Kinter, L. M. Becker, F. Lacbawan, D. Krasnewich, M. Muenke, D. A. Lawrence, M. S. Yerby, C. M. Shaw, B. Gooptu, P. R. Elliott, J. T. Finch, R. W. Carrell, D. A. Lomas, Familial dementia caused by polymerization of mutant neuroserpin. *Nature* **401**, 376–379 (1999).

9. K. J. Kinghorn, D. C. Crowther, L. K. Sharp, C. Nerelius, R. L. Davis, H. T. Chang, C. Green, D. C. Gubb, J. Johansson, D. A. Lomas, Neuroserpin binds Aβ and is a neuroprotective component of amyloid plaques in Alzheimer disease. *J. Biol. Chem.* **281**, 29268–29277 (2006).

10. J. Luo, S. K. T. S. Wärmländer, A. Gräslund, J. P. Abrahams, Non-chaperone proteins can inhibit aggregation and cytotoxicity of Alzheimer amyloid ß peptide. *J. Biol. Chem.* **289**, 27766–27775 (2014).

11. P. Y. Cho, G. Joshi, J. A. Johnson and R. M. Murphy, Transthyretin-derived peptides as β-amyloid inhibitors. *ACS Chem. Nerosci.* **5**, 542–551 (2014).

12. J. Du, P. Y. Cho, D. T. Yang, R. M. Murphy, Identification of beta-amyloid-binding sites on transthyretin. *Protein Eng. Des. Sel.* **25**, 337–345 (2012).

13. N. Jain, J. Ådén, K. Nagamatsu, M. L. Evans, X. Li, B. McMichael, M. I. Ivanova, F. Almqvist, J. N. Buxbaum, M. R. Chapman, Inhibition of curli assembly and *Escherichia coli* biofilm formation

by the human systemic amyloid precursor transthyretin. *Proc. Natl. Acad. Sci. U.S.A.* **114**, 12184–12189 (2017).

14. X. Li, X. Zhang, A. R. A. Ladiwala, D. Du, J. K. Yadav, P. M. Tessier, P. E. Wright, J. W. Kelly, J. N. Buxbaum, Mechanisms of transthyretin inhibition of β-amyloid aggregation in vitro. *J. Neurosci.* **33**, 19423–19433 (2013).

15. H. M. Naylor, M. E. Newcomer, The structure of human retinol-binding protein (RBP) with its carrier protein transthyretin reveals an interaction with the carboxy terminus of RBP. *Biochemistry* **38**, 2647–2653 (1999).

16. S. A. Peterson, T. Klabunde, H. A. Lashuel, H. Purkey, J. C. Sacchettini, J. W. Kelly, Inhibiting transthyretin conformational changes that lead to amyloid fibril formation. *Proc. Natl. Acad. Sci. U.S.A.* **95**, 12956–12960 (1998).

17. G. J. Miroy, Z. H. Lai, H. A. Lashuel, S. A. Peterson, C. Strang, J. W. Kelly, Inhibiting transthyretin amyloid fibril formation via protein stabilization. *Proc. Natl. Acad. Sci. U.S.A.* **93**, 15051–15056 (1996).

18. D. M. Power, N. P. Elias, S. J. Richardson, J. Mendes, C. M. Soares, C. R. A. Santos, Evolution of the thyroid hormone-binding protein, transthyretin. *Gen. Comp. Endocrinol.* **119**, 241–255 (2000).

19. D. T. Yang, G. Joshi, P. Y. Cho, J. A. Johnson, R. M. Murphy, Transthyretin as both a sensor and a scavenger of β-Amyloid oligomers. *Biochemistry* **52**, 2849–2861 (2013).

20. D. Belorgey, D. C. Crowther, R. Mahadeva, D. A. Lomas, Mutant neuroserpin (S49P) that causes familial encephalopathy with neuroserpin inclusion bodies is a poor proteinase inhibitor and readily forms polymers in vitro. *J. Biol. Chem.* **277**, 17367–17373 (2002).

21. K. Barker-Carlson, D. A. Lawrence, B. S. Schwartz, Acyl-enzyme complexes between tissue-type plasminogen activator and neuroserpin are short-lived in vitro. *J. Biol. Chem.* **277**, 46852–46857 (2002).

22. S. C. Goodchild, C. N. Angstmann, S. N. Breit, P. M. G. Curmi, L. J. Brown, Transmembrane extension and oligomerization of the CLIC1 chloride intracellular channel protein upon membrane interaction. *Biochemistry* **50**, 10887–10897 (2011).

23. R. Noto, M. G. Santangelo, S. Ricagno, M. R. Mangione, M. Levantino, M. Pezzullo, V. Martorana, A. Cupane, M. Bolognesi, M. Manno, The tempered polymerization of human neuroserpin. *PLOS ONE* **7**, e32444 (2012).

24. S. Takehara, M. Onda, J. Zhang, M. Nishiyama, X. Yang, B. Mikami, D. A. Lomas, The 2.1-Å crystal structure of native neuroserpin reveals unique structural elements that contribute to conformational instability. *J. Mol. Biol.* **388**, 11–20 (2009).

25. S. Ricagno, S. Caccia, G. Sorrentino, G. Antonini, M. Bolognesi, Human neuroserpin: Structure and time-dependent inhibition. *J. Mol. Biol.* **388**, 109–121 (2009).

26. J. A. Hamilton, L. K. Steinrauf, B. C. Braden, J. Liepnieks, M. D. Benson, G. Holmgren, O. Sandgren, L. Steen, The X-ray crystal structure refinements of normal human transthyretin and the amyloidogenic Val-30 → Met variant to 1.7-Å resolution. *J. Biol. Chem.* **268**, 2416–2424 (1993).

27. P. Mangrolia, D. T. Yang, R. M. Murphy, Transthyretin variants with improved inhibition of β-amyloid aggregation. *Protein Eng. Des. Sel.* **29**, 209–218 (2016).

28. X. Li, J. N. Buxbaum, Transthyretin and the brain re-visited: Is neuronal synthesis of transthyretin protective in Alzheimer's disease? *Mol. Neurodegener.* **6**, 79 (2011).

29. K. Huynh, C. L. Partch. Analysis of protein stability and ligand interactions by thermal shift assay. *Curr. Protoc. Protein Sci.* **79**, 28.9.1–28.9.14 (2015).

30. D. Wu, G. Piszczek, Measuring the affinity of protein-protein interactions on a single-molecule level by mass photometry. *Anal. Biochem.* **592**, 113575 (2020).

31. M. R. Wilson, S. B. Easterbrook-Smith, Clusterin is a secreted mammalian chaperone. *Trends Biochem. Sci.* **25**, 95–98 (2000).

32. D. T. Humphreys, J. A. Carver, S. B. Easterbrook-Smith, M. R. Wilson, Clusterin has chaperone-like activity similar to that of small heat shock proteins. *J. Biol. Chem.* **274**, 6875–6881 (1999).

33. J. J. Yerbury, M. S. Rybchyn, S. B. Easterbrook-Smith, C. Henriques, M. R. Wilson, The acute phase protein haptoglobin is a mammalian extracellular chaperone with an action similar to clusterin. *Biochemistry* **44**, 10914–10925 (2005).

34. K. French, J. J. Yerbury, M. R. Wilson, Protease activation of α_2-macroglobulin modulates a chaperone-like action with broad specificity. *Biochemistry* **47**, 1176–1185 (2008).

35. A. R. Wyatt, J. J. Yerbury, P. Berghofer, I. Greguric, A. Katsifis, C. M. Dobson, M. R. Wilson, Clusterin facilitates in vivo clearance of extracellular misfolded proteins. *Cell. Mol. Life Sci.* **68**, 3919–3931 (2011).

36. J. J. Yerbury, S. Poon, S. Meehan, B. Thompson, J. R. Kumita, C. M. Dobson, M. R. Wilson, The extracellular chaperone clusterin influences amyloid formation and toxicity by interacting with prefibrillar structures. *FASEB J.* **21**, 2312–2322 (2007).

37. P. Narayan, A. Orte, R. W. Clarke, B. Bolognesi, S. Hook, K. A. Ganzinger, S. Meehan, M. R. Wilson, C. M. Dobson, D. Klenerman, The extracellular chaperone clusterin sequesters oligomeric forms of the amyloid-β_{1-40} peptide. *Nat. Struct. Mol. Biol.* **19**, 79–83 (2012).

38. A. R. Wyatt, J. J. Yerbury, M. R. Wilson, Structural characterization of clusterin-chaperone client protein complexes. *J. Biol. Chem.* **284**, 21920–21927 (2009).

39. M. Landreh, A. Rising, J. Presto, H. Jörnvall, J. Johansson, Specific chaperones and regulatory domains in control of amyloid formation. *J. Biol. Chem.* **290**, 26430–26436 (2015).

40. A. Chaari, D. Eliezer, M. Ladjimi, The C-terminal α-helices of mammalian Hsc70 play a critical role in the stabilization of α-synuclein binding and inhibition of aggregation. *Int. J. Biol. Macromol.* **83**, 433–441 (2016).

41. U. Härndahl, B. P. A. Kokke, N. Gustavsson, S. Linse, K. Berggren, F. Tjerneld, W. C. Boelens, C. Sundby, The chaperone-like activity of a small heat shock protein is lost after sulfoxidation of conserved methionines in a surface-exposed amphipathic α-helix. *Biochim. Biophys. Acta* **1545**, 227–237 (2001).

42. C. Visentin, L. Broggini, B. M. Sala, R. Russo, A. Barbiroli, C. Santambrogio, S. Nonnis, A. Dubnovitsky, M. Bolognesi, E. Miranda, A. Achour, S. Ricagno, Glycosylation tunes neuroserpin physiological and pathological properties. *Int. J. Mol. Sci.* **21**, 3235 (2020).

3. R. A. Kammerer, D. Kostrewa, J. Zurdo, A. Detken, C. Garcia-Echeverria, J. D. Green, S. A. Muller, B. H. Meier, F. K. Winkler, C. M. Dobson, M. O. Steinmetz, Exploring amyloid formation by a de novo design. *Proc. Natl. Acad. Sci. U.S.A.* **101**, 4435–4440 (2004).

44. M. R. Wilson, S. B. Easterbrook-Smith, Clusterin binds by a multivalent mechanism to the Fc and Fab regions of IgG. *Biochim. Biophys. Acta* **1159**, 319–326 (1992).

45. X. Liang, L. Peng, K. Li, T. Peterson, F. Katzen, A method for multi-site-directed mutagenesis based on homologous recombination. *Anal. Biochem.* **427**, 99–101 (2012).

46. T. Yokoyama, Y. Kosaka, M. Mizuguchi, Crystal structures of human transthyretin complexed with glabridin. *J. Med. Chem.* **57**, 1090–1096 (2014).

47. L. Whitmore, B. A. Wallace, Protein secondary structure analyses from circular dichroism spectroscopy: Methods and reference databases. *Biopolymers* **89**, 392–400 (2008).

48. L. Whitmore, B. A. Wallace, DICHROWEB, an online server for protein secondary structure analyses from circular dichroism spectroscopic data. *Nucleic Acids Res.* **32**, W668–W673 (2004).

49. D. Cole, G. Young, A. Weigel, A. Sebesta, P. Kukura, Label-free single-molecule imaging with numerical-aperture-shaped interferometric scattering microscopy. *ACS Photonics* **4**, 211–216 (2017).

50. N. R. Cashman, H. D. Durham, J. K. Blusztajn, K. Oda, T. Tabira, I. T. Shaw, S. Dahrouge, J. P. Antel, Neuroblastoma × spinal cord (NSC) hybrid cell lines resemble developing motor neurons. *Dev. Dyn.* **194**, 209–221 (1992).

51. D. Bratosin, L. Mitrofan, C. Palii, J. Estaquier, J. Montreuil, Novel fluorescence assay using calcein-AM for the determination of human erythrocyte viability and aging. *Cytometry A* **66**, 78–84 (2005).

52. J. Zhou, G. Grigoryan, Rapid search for tertiary fragments reveals protein sequence-structure relationships. *Protein Sci.* **24**, 508–524 (2015).